Proceedings of Combustion Institute - Canadian Section
Spring Technical Meeting
Queen's University
May 13-16, 2024

Cycle-to-cycle Variation Quantification of Flow Fields Using Modified Combined Magnitude and Relevance Index

M. Nowruzi* and X. H. Fang

Department of Mechanical and Manufacturing Engineering, Schulich School of Engineering, University of Calgary, 40 Research Place NW, Calgary, AB, Canada, T2L 1Y6

Abstract

Cycle-to-cycle variations (CCV), defined by the inconsistency of combustion events across successive engine cycles despite identical nominal operating conditions, pose a significant challenge to stable operations, thereby limiting potential enhancements in engine efficiency and emissions reduction. Advancements in engine diagnostics have improved the ability to conduct detailed experimental studies on in-cylinder processes' CCV. These investigations have identified key sources of CCV, such as the kinetic energy of the flow field under stoichiometric operating conditions, the interaction between flow and spray in direct-injection spark-ignition (DISI) engines, and specific flow features in particular regions. Quantifying differences in vector fields is required to capture cyclic variations and confirm a successful mitigation in sources of CCV. However, the comparison of vector fields for quantifying cycle-to-cycle variation (CCV) remains a challenge. Vector field comparison, often conducted using metrics like the Relevance Index (RI) and Magnitude Similarity Index (MSI), allows for the quantification of differences between flow fields obtained from experimental measurements and numerical simulations. However, these metrics can yield misleading results in comparison of vector fields having relatively high varying velocity magnitude areas, such as areas near the vortex centers of in-cylinder turbulent flows. In addition, their high dependency on velocity magnitude can also result in a misleading focus on low-velocity magnitude areas. Previous works have introduced normalized metrics such as the Weighted Relevance Index (WRI) and the Weighted Magnitude Index (WMI), and their combination as the Combined Magnitude and Relevance Index (CMRI) with less sensitivity to such areas. However, CMRI, as a method for combining WRI and WMI, does not consider their significance equally, which can lead to errors in comparison of vector fields. In this paper, a comparison of advanced metrics used for comparing vector fields is detailed using the PIV experimental data from the Darmstadt engine. Furthermore, an improved version of the CMRI as modified CMRI is introduced, and its applicability and preference for quantifying cyclic variation have been investigated. Overall, the improved combined metric is found to provide a more robust quantification of the differences between flow fields, making it a suitable candidate for the quantification of CCV in engine flow fields.

1 Introduction

Comparison between different experimentally and numerically generated data has many applications for both validating new numerical models and measurement techniques [1][2][3][4]. Research in fields such as internal combustion engines (ICEs), oceanography, and biomedical engineering devices requires an accurate understanding of flow fields. In these applications, vector fields obtained from particle image velocimetry (PIV) measurements are often used to validate simulations from computational fluid dynamics (CFD) [1, 5]. As comparing vector fields is often needed, quantitative metrics to robustly compute the differences between flow fields have been investigated.

Among others, the Relevance Index (RI) has been widely used in various applications for vector alignment comparison, serving as a valuable tool in the investigation of LES simulations' convergence for engine studies. It is dependent on the vector elements' values and, thus, on the magnitudes of the compared vector fields. Consequently, changes in vector field magnitude will alter RI's value unless all vectors in a vector field are multiplied by a real number. The RI index has been employed to quantify differences in spray characteristics [6][7] and proper orthogonal decomposition (POD) modes derived from PIV measurements [8][9].

*Corresponding author: muhammad.nowruzi@ucalgary.ca

For vector fields' magnitude comparison, the Magnitude Similarity Index (MSI) has been applied to explore the alignment of simulated OH mass proportion and particulate matter mass proportion distributions in an n-dodecane spray flame [10] and to assess discrepancies in the flow field between simulations and experimental results [11][12]. In a study of valve vibration effects on intake air flow in an IC engine, the Local Magnitude Index (LMI) and Local Structural Index (LSI), the local versions of MSI and RI, have been applied to measure the difference between PIV-measured velocity fields at three different valve lifts [13]. Notably, LSI does not have a dependency on the magnitude of two local vectors being compared and has the same range as RI. The spatially averaged value of the LSI field is not equal to the RI unless two vector fields are strictly proportional [14]. Despite LSI and LMI benefits, they can still result in errors when implementing them to make comparisons in some low-velocity magnitude areas, such as tumble motion in internal combustion engines. To improve LSI, the LSI equation is multiplied by a normalization factor with dependency on magnitude so that it increases and decreases the magnitude of LSI in high and low velocity regions, respectively [1]. In the case of LMI, the issue of sensitivity to extremum velocity magnitudes is mitigated by using global median velocity magnitude instead of local velocity magnitude in the denominator of the LMI equation. Improved versions of LMI and LSI, specifically for engine research, are Weighted Magnitude Index (WMI) and Weighted Relevance Index (WRI), respectively [1]. In engine research, they have been used to qualitatively compare the similarity of reconstructed flow fields using kernel principal component analysis (KPCA) with Reynolds Average Navier-Stokes (RANS) simulations [14].

Combined metrics, which integrate WRI and WMI, demonstrate differences in flow fields through alignment and magnitude disparities. These metrics, useful for comprehensive comparisons, provide a scalar average to highlight the significance of differences between two flow fields. When used alongside a benchmark, they assess the accuracy of data from simulations or experiments. The robustness of these methods, crucial for their efficacy, depends on the scaling technique used to merge WMI and WRI. Unlike the traditional Combined Magnitude and Relevance Index (CMRI), which may bias towards one metric, the proposed modified CMRI treats WRI and WMI equally, thus, establishing a foundation for developing various scaling methods.

In this study, the accuracy and robustness of comparison indexes for quantifying the vector differences for the Damstart engine PIV flow fields are detailed. First, the details of each above-mentioned metric are introduced, and their accuracy is studied on the experimental data. Both the shortcomings and advantages of each method are discussed. Finally, a new scaling method resulting in a modified CMRI is introduced, and the merit of this approach is highlighted.

2 Experimental Data

This study utilizes PIV measurements from the Darmstadt engine, a single-cylinder engine with optical access as detailed in [15]. The dataset comprises 250 snapshots of consecutive engine cycles taken on the valve plane, offset from the cylinder center to align with the intake valves. Measurements were captured every five crank angle degrees (CAD) from 360 to 720 CAD after firing the top dead center (aTDCf), with a focus on phases at 470 and 700 CAD aTDCf. These phases were chosen to observe critical engine phenomena, such as intake valve behavior and fuel-air mixing before combustion. The time interval between consecutive images was 0.15 seconds, providing insights into the intricate flow dynamics within the combustion chamber under specific operating conditions. The subset of measurements done at 470 CAD has been used in the current study.

3 Quantitative metrics

In this section, a brief description of each quantitative metric to be tested is given, starting with the metrics for vector alignment difference, followed by the vector magnitude difference, and the overall vector field differences. The discrete two-dimensional velocity field data sets usually obtained from PIV measurements or CFD simulations consist of ordered pairs of the form (u, v) for each velocity vector $\boldsymbol{q}$ associated with a data point (x_i, z_j) in the discrete flow field, where u and v are velocity components along two perpendicular axes. The vector magnitude is defined as the L^2 norm $\|\boldsymbol{q}\|_2$, and angle θ is defined by the definition of the dot product between vectors, having set a reference direction.

3.1 Vector Fields' Alignment Difference

Standard RI, using the definition of the angle between two high-dimensional vectors, is capable of showing an overall alignment agreement between two vector fields with the same number of elements. Using RI, defined as

[16],

$$\mathrm{RI} = \frac{\boldsymbol{q}_\mathrm{A} \cdot \boldsymbol{q}_\mathrm{B}}{\|\boldsymbol{q}_\mathrm{A}\|_2 \|\boldsymbol{q}_\mathrm{B}\|_2} = \cos\left(\theta_\mathrm{AB}\right), \tag{1}$$

for the alignment comparison of two dimensional vector fields, the $\cos\left(\theta_\mathrm{AB}\right)$, where $\theta_\mathrm{AB} = |\theta_\mathrm{A} - \theta_\mathrm{B}|$, is being calculated. The vector $\boldsymbol{q}_\mathrm{A}$ included in the dot product, $\boldsymbol{q}_\mathrm{A} \cdot \boldsymbol{q}_\mathrm{B}$, is of dimensions $2 \times N$, with N representing the number of vectors in the vector field A, and the number 2 denoting the two elements of each vector in a two dimensional vector field. RI assigns values in the range $[-1, 1]$, with higher values associated with the better alignment agreement between two compared vectors.

To have local comparison between alignment of vector fields, local structural index (LSI) defined as,

$$\mathrm{LSI}\left(x_i, z_j\right) = \frac{\boldsymbol{q}_\mathrm{A}(x_i, z_j) \cdot \boldsymbol{q}_\mathrm{B}(x_i, z_j)}{\|\boldsymbol{q}_\mathrm{A}(x_i, z_j)\|_2 \|\boldsymbol{q}_\mathrm{B}(x_i, z_j)\|_2} = \cos\left(\theta_\mathrm{AB}(x_i, z_j)\right), \tag{2}$$

is used. The location (x_i, z_j) is associated with the same point in the two compared vector fields. In the LSI equation, the $\cos\left(\theta_\mathrm{AB}(x_i, z_j)\right)$, where $\theta_\mathrm{AB}(x_i, z_j) = |\theta_\mathrm{A}(x_i, z_j) - \theta_\mathrm{B}(x_i, z_j)|$ is being computed, and the results are usually shown as contour plots providing information about the local alignment difference between the two vector fields being compared.

Improving LSI to avoid velocity magnitude sensitivity, a new metric named weighted relevance index (WRI) has been introduced as [1],

$$\mathrm{WRI}\left(x_i, z_j\right) = \left(\frac{1 - \mathrm{LSI}\left(x_i, z_j\right)}{2}\right)\left(\frac{\|\boldsymbol{q}_\mathrm{A}(x_i, z_j)\|_2 \, \|\boldsymbol{q}_\mathrm{B}(x_i, z_j)\|_2}{\mathrm{median}(\boldsymbol{Q}_\mathrm{A}) \ \mathrm{median}(\boldsymbol{Q}_\mathrm{B})}\right), \tag{3}$$

where the $\boldsymbol{Q}_\mathrm{A}$ is the magnitude field of the vector field A. Making comparisons using WRI results in a zero value for vectors with the same alignment and a value of 0.5 for two perpendicular vectors, with their magnitudes, in both vectors, equal to the median magnitude of their own flow field [1].

3.2 Vector Fields' Magnitude Difference

Quantifying differences in magnitude is also essential when comparing two flow fields [1]. magnitude similarity index (MSI) (also called global magnitude index (GMI)[17]) and its local version, local magnitude index (LMI), are the first metrics dependent on the magnitude of vectors in the literature [16].

$$\mathrm{MSI} = 1 - \frac{\|\boldsymbol{q}_\mathrm{A} - \boldsymbol{q}_\mathrm{B}\|_2}{\|\boldsymbol{q}_\mathrm{A}\|_2 + \|\boldsymbol{q}_\mathrm{B}\|_2} \tag{4}$$

$$\mathrm{LMI} = \frac{|\boldsymbol{Q}_\mathrm{A}(x_i, z_j) - \boldsymbol{Q}_\mathrm{B}(x_i, z_j)|}{\boldsymbol{Q}_\mathrm{A}(x_i, z_j) + \boldsymbol{Q}_\mathrm{B}(x_i, z_j)} \tag{5}$$

The MSI and LMI produce values from 0 to 1, with lower values correlated to better magnitude agreement in MSI and the reverse for LMI [1]. The MSI , through the vector subtraction in its nominator, is dependent on both magnitude and direction [1].

Weighted magnitude index (WMI) defined as [1],

$$\mathrm{WMI}(x_i, z_j) = \frac{|\boldsymbol{Q}_\mathrm{A}(x_i, z_j) - \boldsymbol{Q}_\mathrm{B}(x_i, z_j)|}{\mathrm{median}(\boldsymbol{Q}_\mathrm{A}, \boldsymbol{Q}_\mathrm{B})} \tag{6}$$

was introduced as an alternative for LMI by changing its normalization factor from summation of vector magnitudes to median vector magnitude of both compared flow fields [1].

3.3 Vector Fields' Overall Difference

Comparing the magnitude and alignment of flow fields solely through the use of WRI and WMI is not desirable, as low WRI and WMI are not related to each other, and an overall comparison based on using only one of them is not valid [1]. Therefore, the combined magnitude and relevance index (CMRI) has been introduced as [1],

$$\mathrm{CMRI}(x_i, z_j) = \frac{\mathrm{WMI}_{(norm)}(x_i, z_j) + \mathrm{WRI}_{(norm)}(x_i, z_j)}{2} \tag{7}$$

to ease a valid comparison between two vector fields [1]. Trying to define the CMRI, a trivial average of WRI and WMI, (WRI + WMI)/2, failed to capture the differences, simultaneously, in magnitude and alignment through the difference in distribution of WMI and WRI, which can be addressed by their normalization [1]. Normalization is done so that the majority of WRI and WMI values lie between 0 and 1, so the top and bottom 2% percentile of values in both WRI and WMI results are used for the scaling [1].

$$\mathrm{WRI}_{(norm)}(x_i, z_j) = \frac{\mathrm{WRI}(x_i, z_j) - \mathrm{WRI}_{(2\%)}}{\mathrm{WRI}_{(98\%)} - \mathrm{WRI}_{(2\%)}} \tag{8}$$

The CMRI index captures dissimilarities in both magnitude and alignment and, therefore, has given a reasonable meaning for spatially averaged CMRI as a number indicating the overall agreement of two vector fields [1]. However, the proposed scaling method for CMRI does not consider the significance of the two metrics the same. In order to fulfill this requirement, a new scaling method is introduced as,

$$\text{modified CMRI}(x_i, z_j) = \frac{\frac{\mathrm{WMI}(x_i, z_j)}{\max(\mathrm{WMI})} + \frac{\mathrm{WRI}(x_i, z_j)}{\max(\mathrm{WRI})}}{2}, \tag{9}$$

which is capable of capturing the maximum values of both metrics. Unlike CMRI, with its upper bound dependent on the vector magnitudes of compared vector fields, modified CMRI has a fixed upper bound. Modified CMRI gives values in the range [0, 1], the 0 value for comparing two identical vectors, and the value 1 for the case in which a vector is being compared to a zero magnitude vector.

4 Results

Non-reacting flow studies are essential for the study of in-cylinder air/fuel mixing behaviors. The main source of kinetic energy in these flow fields is typically the high-speed intake jet entering from the top section of the cylinder. Fluctuations in the intake jet's main-stream direction are the core factor that governs the variation between different engine cycles' flow fields. The first step towards understanding the effects of cyclic variation on the in-cylinder flow field and, hence, on engine performance is developing methods to quantify the variations between the flow fields. These methods enable determining the range of the variation from the ensemble mean for a data set and can also be applied to validate the simulated flow fields with experimental measurements. Generally, the methods for comparison of vector fields are divided into three categories, as discussed in Section 3. In what follows, the application of these methods for comparing two single flow fields will be discussed.

The first point-wise alignment comparison method used is LSI, which computes the cosine of the angle between two vectors. Implementing LSI for comparing flow fields' alignment might lead to wrong conclusions when comparing flow fields containing regions with vectors with relatively low magnitudes. This is usually the case when analyzing turbulent flows through their vortices, which contain the lowest velocity magnitudes in the vicinity of their centers. In the case of ICEs, tumble motion created by the intake jet and intensified by piston motion results in vortices with low velocity magnitudes near their centers [18]. Due to cycle-to-cycle variation in internal combustion (IC) engines, the vortex center in different cycles varies with each other. It has been shown that using LSI to compare two 150 cycle-averaged flow fields from the same crank angle (CA) leads to the observation of large differences around their vortex centers, which originated from the higher relative change in alignment of velocities towards vortex centers [1]. Comparing the two different 10-cycle averaged flow fields from our dataset in Figs. 1(a) and 1(b) shows how vortex center displacement and low velocity magnitude areas result in large differences between two similar vector fields when compared by LSI (the white dashed circles in Fig. 1(c)). As suggested by previous studies, in cases where there are a large number of snapshots to be analyzed, comparing the spatially averaged LSI of two flow fields is preferable to a one-by-one comparison between LSI contour plots. In these cases, the large unwanted differences will control the spatially averaged LSI and hide the relatively low alignment differences in high-velocity regions of the flow [1].

As discussed in the previous section, a simple way to address the LSI issue with low-velocity regions is to include local velocity magnitudes in its equation to weight the cosine of the angles between two vectors with the vectors' magnitudes. Comparison between WRI (Fig. 1(d)) and LSI (Fig. 1(c)) contour plots has shown that unlike the LSI, WRI can capture misalignments in the higher velocity magnitude regions of the flow field, as well as misalignments in the lower velocity magnitude regions near the vortex centers [1]. The implementation of WRI has resulted in reducing focus on the low velocity magnitude areas (white dashed circles in Fig. 1(d)) and highlighting a region with higher velocity magnitude (green dashed circle in Fig. 1(d)). WRI highlights the

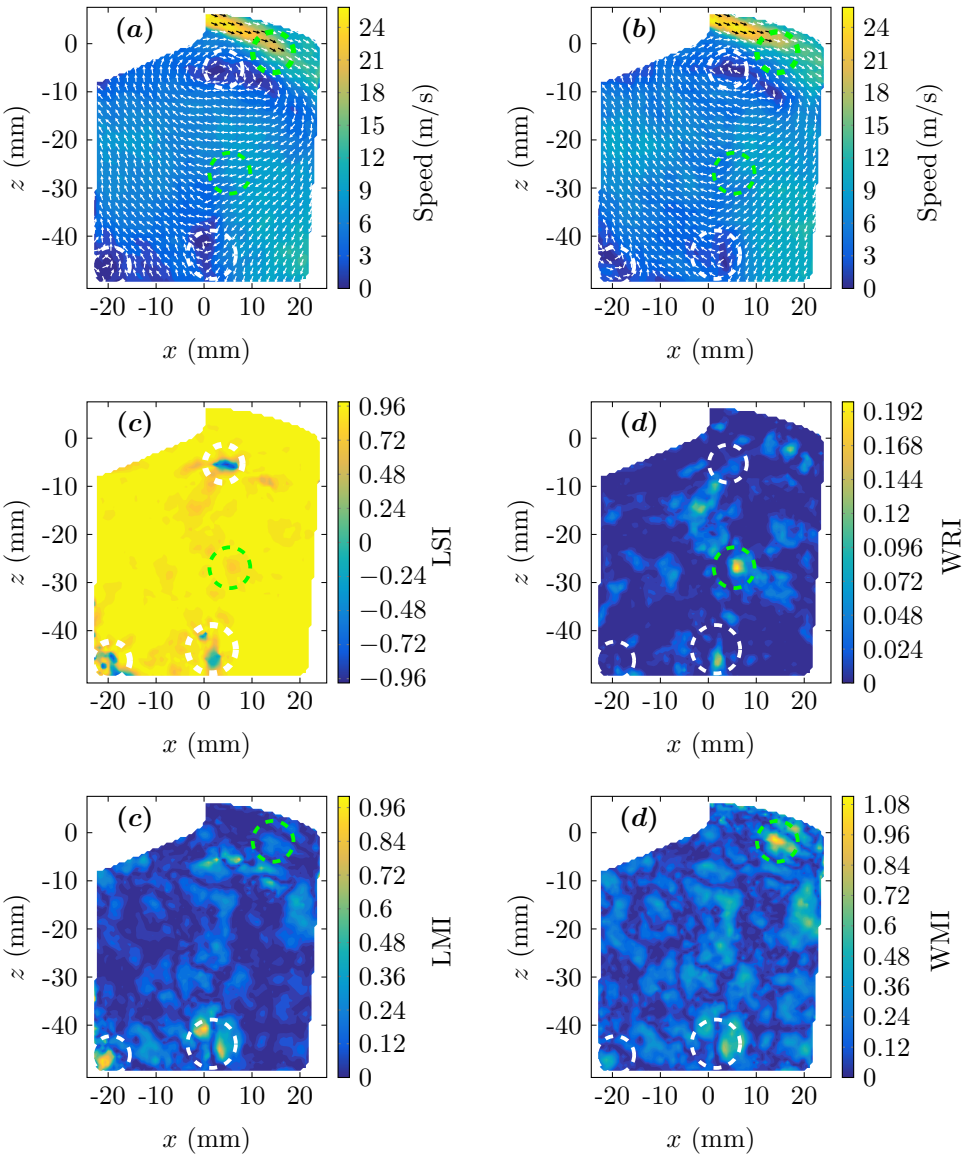

Fig. 1: Comparison of two different 10-cycle PIV dataset averaged flow fields **(*a*)** and **(*b*)**, using **(*c*)** LSI, **(*d*)** WRI, **(*e*)** LMI, and **(*f*)** WMI methods.

areas with different alignments that contain more kinetic energy in the two compared flow fields. Therefore, spatially averaged WRI, unlike spatially averaged LSI, is a more reliable characterization of the alignment variation between the two compared flow fields. The same improvement in the maximum regions assigned by WMI in comparison to LMI is recognized by comparing their contour plots in Figs. 1(e) and 1(f), respectively. Using WMI has led to capturing a high-speed region along the main stream of the intake jet (the green dashed circle in Fig. 1(f)) that cannot be seen by using LMI.

To see the differences captured by both WRI and WMI, combined metrics are used. The combined metrics show the difference between flow fields as a combination of alignment and magnitude difference. Since these metrics are capable of making an overall comparison, their spatially averaged value can be used as a scalar showing the significance of the difference between two flow fields. Comparing with a benchmark case, combined metrics can evaluate the accuracy of a dataset obtained from simulations or experiments. As these methods are capable of performing evaluation, their robustness is of great importance, which is related to the scaling method they use to combine WMI and WRI. To show how modified CMRI improves CMRI by changing the scaling method for combining WRI and WMI, cycles 17 and 28 of our dataset have been chosen. When implementing WRI

and WMI to compare cycles 17 and 28, the regions with the maximum value in the WRI and WMI contour plots have different locations (Fig. 2(a) and 2(b)). This makes it possible to see the difference between our proposed scaling method and the previous one for combining WRI and WMI. Since the CMRI contour plot itself is not intuitive enough as it is a combination of magnitude and alignment difference, showing the WRI and WMI contour plots would also give a clearer view of the vector fields [1]. CMRI and modified CMRI have been used, respectively, to combine WRI and WMI metrics (Figs. 2(c) and 2(d)). The maximum values of the WMI and WRI fields are the maximum values captured by the modified CMRI field. In comparison to CMRI, which does not consider the significance of WRI and WMI equally, modified CMRI treats both metrics the same. As this approach defines how we can combine two metrics equally, it results in a baseline that enables further development of different scaling methods. In future work, spatially averaged modified CMRI will be used to capture the cyclic variation throughout a dataset with respect to its ensemble mean.

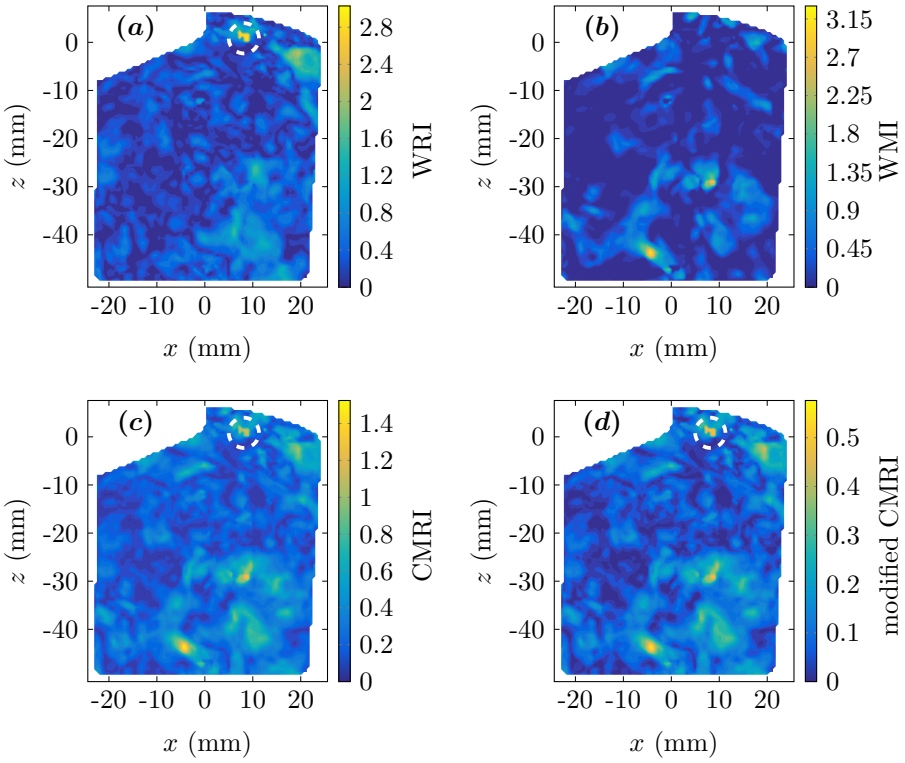

Fig. 2: Comparison of cycles 17 and 28 using **(*a*)** WMI, **(*b*)** WRI, **(*c*)** CMRI and **(*d*)** modified CMRI.

5 Conclusion

The CMRI, WRI, WMI, LSI, and LMI metrics each offer distinct advantages and are recommended for application based on their properties, preferably in conjunction with complementary flow characterization methods like vortex tracking [1][19]. The WRI, WMI, and CMRI demonstrate sensitivity to differences in both high and low velocity regions within a flow field. In cases where relative changes in low velocity regions hold critical significance or when any type of velocity weighting is undesirable, the LSI and LMI metrics are more suitable alternatives. Discussing the scaling issue in the original CMRI index, a new method for more robustly capturing the overall differences among two vector fields is proposed and used to capture variation between two different cycles. Further work can be done to relate the quantitative metrics to the scales of the motion in specific flow conditions, such as slender flows, in order to reach a threshold under which the significance of similarity between two vector fields can be defined and used for validation of simulation data with experimental measurements.

Acknowledgments

We gratefully acknowledge the financial support provided by the Natural Sciences and Engineering Research Council of Canada and Alberta Innovates. The authors also want to thank the DARMSTADT Research Group for providing experimental data. We also acknowledge Prof. Stefano Fontanesi for inspiring the inception of this research.

References

[1] C. Willman, B. Scott, R. Stone, D. Richardson, Quantitative metrics for comparison of in-cylinder velocity fields using particle image velocimetry, Experiments in Fluids 61 (2020) 1–16.

[2] F. Hernández-Jiménez, S. Sánchez-Delgado, A. Gómez-García, A. Acosta-Iborra, Comparison between two-fluid model simulations and particle image analysis & velocimetry (PIV) results for a two-dimensional gas–solid fluidized bed, Chemical engineering science 66 (17) (2011) 3753–3772.

[3] R. A. Malinauskas, P. Hariharan, S. W. Day, L. H. Herbertson, M. Buesen, U. Steinseifer, K. I. Aycock, B. C. Good, S. Deutsch, K. B. Manning, et al., FDA benchmark medical device flow models for CFD validation, Asaio Journal 63 (2) (2017) 150–160.

[4] S. J. Baker, X. H. Fang, A. Barbato, S. Breda, M. Magnani, S. Fontanesi, F. C. P. Leach, M. H. Davy, Extracting vector magnitudes of dominant structures in a cyclic engine flow with dimensionality reduction, Physics of Fluids 36 (2) (2024) 025131.

[5] S. Baker, X. Fang, L. Shen, C. Willman, J. Fernandes, F. Leach, M. Davy, Dynamic mode decomposition for the comparison of engine in-cylinder flow fields from particle image velocimetry (PIV) and Reynolds-averaged Navier–Stokes (RANS) simulations, Flow, Turbulence and Combustion (2023) 1–26.

[6] H. Chen, D. L. Hung, M. Xu, J. Zhong, Analyzing the cycle-to-cycle variations of pulsing spray characteristics by means of the proper orthogonal decomposition, Atomization and Sprays 23 (7) (2013).

[7] H. Chen, M. Xu, D. L. Hung, Analyzing in-cylinder flow evolution and variations in a spark-ignition direct-injection engine using phase-invariant proper orthogonal decomposition technique, Tech. rep., SAE Technical Paper (2014).

[8] H. Chen, D. L. Reuss, V. Sick, On the use and interpretation of proper orthogonal decomposition of in-cylinder engine flows, Measurement Science and Technology 23 (8) (2012) 085302.

[9] H. Chen, D. L. Reuss, D. L. Hung, V. Sick, A practical guide for using proper orthogonal decomposition in engine research, International Journal of Engine Research 14 (4) (2013) 307–319.

[10] M. M. Ameen, Y. Pei, S. Som, Computing statistical averages from large eddy simulation of spray flames, Tech. rep., SAE Technical Paper (2016).

[11] M. M. Ameen, X. Yang, T.-W. Kuo, S. Som, Using LES to simulate cycle-to-cycle variability during the gas exchange process, in: Internal Combustion Engine Division Fall Technical Conference, Vol. 58325, American Society of Mechanical Engineers, 2017, p. V002T06A015.

[12] N. Van Dam, W. Zeng, M. Sjöberg, S. Som, Parallel multi-cycle LES of an optical pent-roof DISI engine under motored operating conditions, in: Internal Combustion Engine Division Fall Technical Conference, Vol. 58325, American Society of Mechanical Engineers, 2017, p. V002T06A019.

[13] F. Shi, M. Liu, D. L. Hung, X. Li, M. Xu, Valve vibration induced intake air flow dynamics analysis using near valve particle image velocimetry, Journal of Engineering for Gas Turbines and Power 144 (9) (2022) 091004.

[14] X. Fang, L. Shen, C. Willman, R. Magnanon, G. Virelli, M. H. Davy, R. Stone, Manifold reduction techniques for the comparison of crank angle-resolved particle image velocimetry (PIV) data and Reynolds-averaged Navier-Stokes (RANS) simulations in a spark ignition direct injection (SIDI) engine, International Journal of Engine Research 23 (8) (2022) 1275–1294.

[15] E. Baum, B. Peterson, B. Böhm, A. Dreizler, On the validation of LES applied to internal combustion engine flows: part 1: comprehensive experimental database, Flow, turbulence and combustion 92 (2014) 269–297.

[16] K. Liu, D. C. Haworth, Development and assessment of POD for analysis of turbulent flow in piston engines, Tech. rep., SAE Technical Paper (2011).

[17] F. Zhao, M. Liu, P. Ge, D. L. Hung, X. Li, M. Xu, X. Yang, C. Idicheria, Multi-plane time-resolved particle image velocimetry (PIV) flow field measurements in an optical spark-ignition direct-injection (SIDI) engine for large-eddy simulation (LES) model validations, Oil & Gas Science and Technology–Revue d'IFP Energies nouvelles 74 (2019) 52.

[18] R. Stone, Introduction to internal combustion engines, Vol. 3, Springer, 1999.

[19] C. Simpson, H. Babinsky, J. Harvey, S. Corkery, Detecting vortices within unsteady flows when using single-shot PIV, Experiments in Fluids 59 (8) (2018) 1–13.